3X DC-DC Multiplier/Divider for HEV Systems

Wei Qian, Fang Z. Peng, Miaosen Shen
Michigan State University,
2120 Engineering Building,
East Lansing, MI, 48824

Leon M. Tolbert
University of Tennessee, Knoxville, TN
Electrical Engineering and Computer Science,
Knoxville, Tennessee, 37996

***Abstract*- This paper presents a bidirectional 3X dc-dc multiplier/divider that can interface the battery with the inverter dc bus for hybrid electric vehicle (HEV) traction drives. Compared with traditional multi-level dc-dc converter, this converter can have three output/input voltage ratios with smooth transition. The control method to limit the transient inrush current, as well as a novel regenerative clamping circuit for multi-level dc-dc converters is provided in this paper. By utilizing the parasitic inductance or the minimum inductance from an air core inductor, the size and weight of the converter can be significantly reduced. Its magnetic-less feature and high efficiency provide the potential of the high temperature operation with the future wide bandgap devices. Experimental results are given to verify the operating principle and the design concepts of this topology.**

I. INTRODUCTION

Power converters play a vital role in Hybrid Electric Vehicle (HEV) systems. Typical HEV drive train consists of a battery, power converter, and a traction motor to drive the vehicle. The power converter could be just a traditional inverter or a dc-dc converter plus an inverter. The latter configuration provides more flexibility and improves the system performance. The dc-dc converter in this system interfaces the battery and the inverter dc bus, which is usually a variable voltage converter so that the inverter can always operate at its optimum operating point. In most commercially available systems, traditional boost converters are used. In this system, the inductor is bulky, heavy, costly, and always one of the hottest components. With the trend of higher coolant temperature of the converters in HEVs, as the only power magnetic component in the system, the dc-dc inductor becomes a major obstacle to further reducing the size, weight, and cost.

Multi-level dc-dc converters become attractive for this application because of the magnetic-less structure. With the development of the wide bandgap device and high temperature multilayer ceramic capacitors, the multi-level dc-dc converters becomes a good candidate for very high temperature operation (>250^{o}C), which may eliminate coolant and further reduce cost. Traditional multi-level dc-dc converters (switched capacitor converters) usually have fixed input and output voltage ratio. This paper presents a bidirectional 3X dc-dc multiplier/divider that is able to achieve three different output/input voltage ratios by proper control. Thus, the inverter can always operate close to its optimum operation point.

II. OPERATION PRINCIPLE

The presented 3X dc-dc multiplier/divider shown in Fig.1 employs the same topology as in literature [1]; however with proper control, it can have three voltage ratios instead of fixed 3:1 shown in [1]. With three different PWM methods, the output voltage ratio Vout/Vin can be 1, 2, or 3 in steady state. Because of its bi-directional nature, the converter can be viewed as a multiplier or a divider based on the definition of source and load.

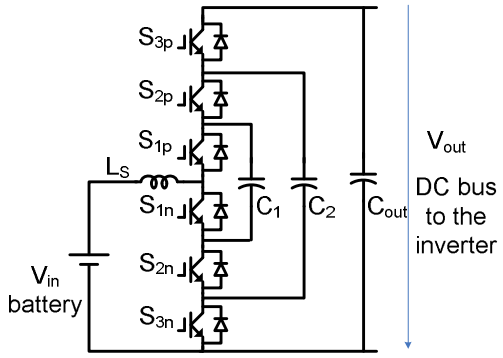

Fig.1. Topology of the 3X dc-dc multiplier/divider

1X: To achieve the voltage ratio of 1, namely 1X, the converter always operates in one switching state as shown in Fig.2, with all the switches (IGBTs with freewheeling diodes) except S_{1n} always turned on. Thus, all the capacitors are connected in parallel with the input voltage, which ensures the voltage ratio of 1.

2X: While C_2 and C_{out} are always paralleled by S_{3p} and S_{3n}, the converter alternates with 1/2 duty ratio between two switching states I and II illustrated in Figs.3 (a) and (b). In state I, the capacitor C_1 is connected to the battery; in state II, C_1 is in series with the battery to connect to C_2 and C_{out}. Consequently, the voltage ratio will be kept to 2X.

3X: When the desired ratio is 3X, the converter circulates from switching states I, II to III as shown in Figs.4 (a), (b) and (c), with 1/3 duty ratio per state. In State I, $V_{c1}=V_{in}$; in state II, $V_{c2}=V_{c1}+V_{in}$; in State III, $V_{c3}=V_{c2}+V_{in}$. After these three states, the capacitor voltages will be balanced automatically. As a result, the output voltage is three times the input voltage.

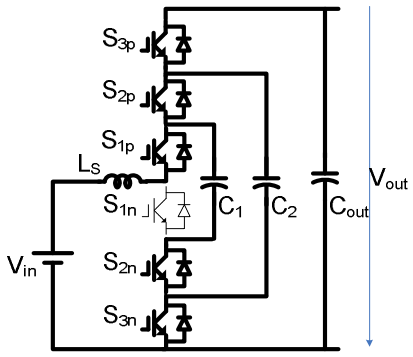

Fig. 2. Switching patterns for 1X mode

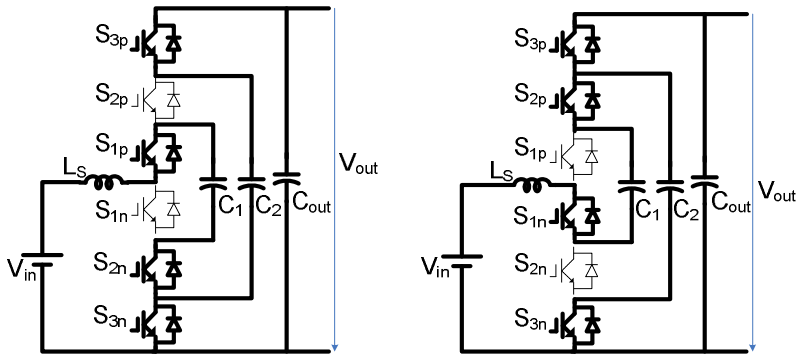

(a) (b)

Fig. 3. Switching patterns for 2X mode: (a) Switching state I. (b) Switching state II.

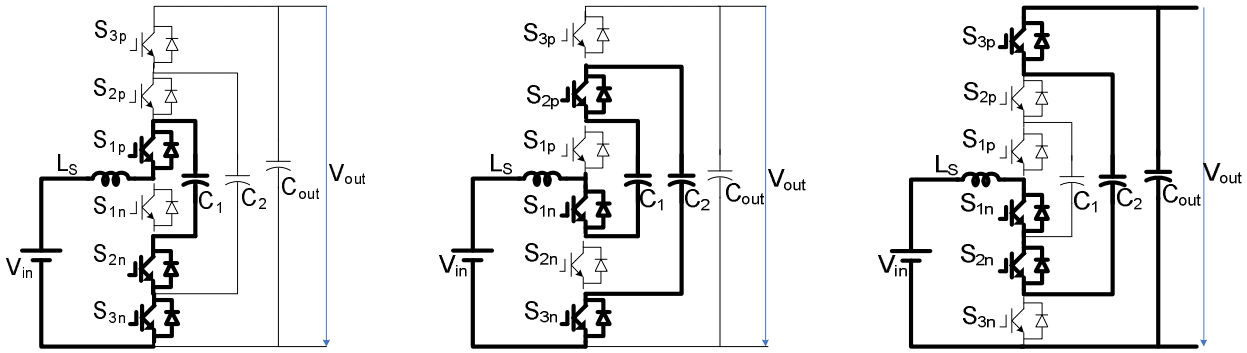

(a) (b) (c)

Fig.4. Switching patterns for 3X mode. (a) Switching state I. (b) Switching state II. (c) Switching state III.

III. Transient Current Control during Transition

In the steady state, the capacitor voltages are well balanced and the voltage differences are very small, so the current through the switches is relatively small. However, during the transition when the output voltage ratio changes between V_{in} and $2V_{in}$, or between $2V_{in}$ and $3V_{in}$, the voltage differences are very large, which can lead to high transient current through the devices and capacitors. Therefore, a variable PWM duty ratio and high switching frequency is indispensable in transition in order to limit the transient current. Furthermore, a small air-core inductor can be added when parasitic inductance is not enough for the large voltage difference and the adopted devices can not achieve sufficiently high switching frequency.

A. Changing the output voltage from $1V_{in}$ to $2V_{in}$

Before changing the output voltage from $1V_{in}$ to $2V_{in}$, all the three capacitors are initially charged to $1V_{in}$ in 1X mode. After the transition, the capacitors C_2 and C_{out} should be charged up to $2V_{in}$. Assume that the aforementioned inductor current is continuous and define duty ratio D as of the time when C_{out} is charged by the addition of C_1 and the battery over the entire switching period T_s. There are two active switching states and one freewheeling state between them. In the active switching states, the gate signals are given in sequence to the switches as shown in Figs. 3(a) and (b) of the 2X steady state operation, except that the duty ratio D increases gradually. To balance the voltage across C_1, the duty ratios of the two switching states I and II are assigned equal. In the freewheeling state shown in Fig. 5, the switches S_{2p}, S_{1p}, S_{1n} and S_{2n} are all given the turn-off gate signals, therefore, the continuous current goes through the freewheeling diodes inside S_{1p} and S_{2p}. So the middle point voltage V_m equals V_o for a duration of $(1/2–D)T_s$ after each active state. According to the inductor voltage-second balance in steady state, the relationship of the input voltage with output voltage and duty cycle is:

$$V_{in} = DV_{c1} + D(V_{out} - V_{c1}) + 2(\frac{1}{2} - D)V_{out} = (1-D)V_{out} \quad (1)$$

From the steady state boundary condition of 1X and 2X modes, the duty cycle should vary from 0 to 1/2 to change the output smoothly to $2V_{in}$. The PWM signals are shown in Fig. 6.

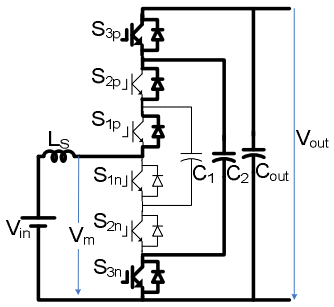

Fig. 5. The freewheeling state in the 1X to 2X transition

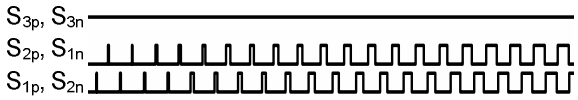

Fig.6. PWM signals during the transition from 1X to 2X

B. *Changing the output voltage from $2V_{in}$ to $3V_{in}$*

Applying the same principle to the transition from $2V_{in}$ to $3V_{in}$, there are three active switching states and three freewheeling states shown in Fig. 7 among them. The duration is DT_s for each active state and $(1/3–D)T_s$ for each freewheeling state. In the active switching states, the PWM signals in Fig. 8 are given to the corresponding switches as shown in Figs. 4(a), (b) and (c) of the 3X steady state operation. In the freewheeling state shown in Fig. 7(a), since only S_{3n} is kept on after State I in Fig. 4(a), the continuous current freewheels through the diodes inside S_{1p} and S_{2p} and thereby V_m equals V_{c2}; in Fig. 7 (b), V_m equals $V_{out}–V_{c1}$ due to the freewheeling; in Fig. 7(c), V_m equals $V_{out}–V_{c2}+V_{c1}$. Hence, the relationship of the input and output voltages can be derived as:

$$V_{in} = (\frac{2}{3} - D)V_{out} \tag{2}$$

From the boundary condition, the ideal duty cycle varies from 1/6 to 1/3 in the transition.

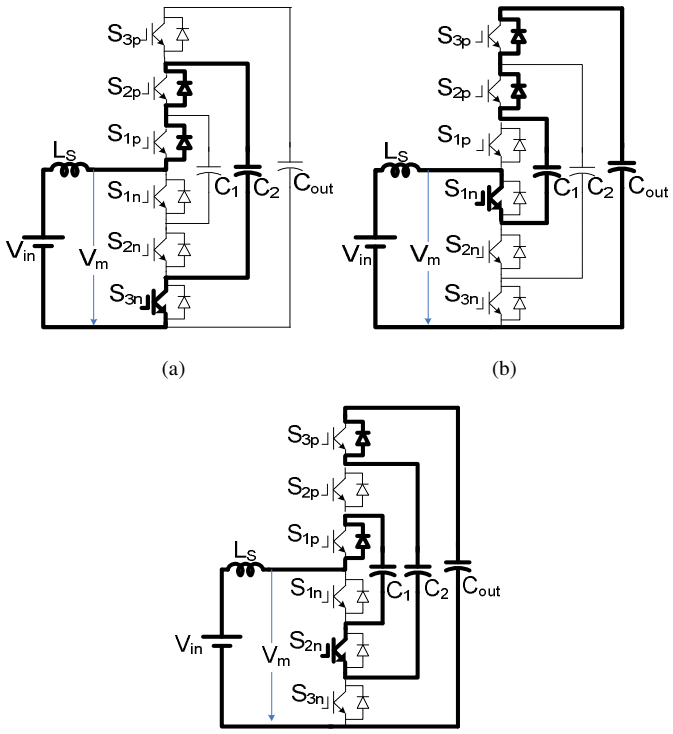

Fig. 7. The freewheeling states in the 2X to 3X transition: (a) Freewheeling after the active switching state I in Fig. 4(a). (b) Freewheeling after the active switching state II in Fig. 4(b). (c) Freewheeling after the active switching state III in Fig. 4(c).

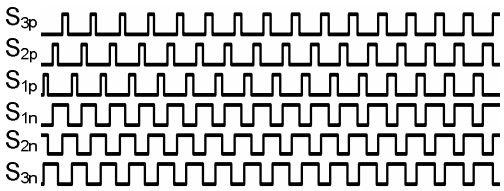

Fig.8. PWM signals during the transition from 2X to 3X

C. *Changing the output voltage from $3V_{in}$ to $2V_{in}$*

The control strategy for the $3V_{in}$ to $2V_{in}$ transition is to maintain the first two switching patterns in 3X mode as shown in Figs. 4 (a) and (b) for 1/2 duty ratio. After the output capacitor C_{out} is naturally discharged by the load and its voltage goes down to below the voltage of C_2, there will be no oscillation when S_{3p} is switched on as shown in Fig. 8. In consequence, the converter settles down to the 2X mode bidirectional steady state operation as shown in Figs. 3 (a) and (b).

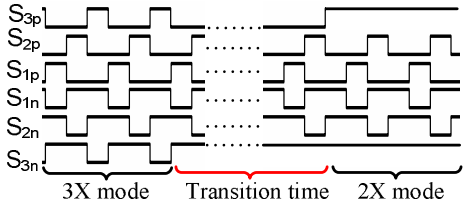

Fig.9. PWM signals during the transition from 3X to 2X

D. *Changing the output voltage from $2V_{in}$ to $1V_{in}$*

Similarly, during the transition from 2X to 1X, the switching state of the converter is the same as the switching state shown in Fig. 4(a). That is, the gate signals illustrated in Fig. 10 are applied to only keep S_{1p}, S_{2n} and S_{3n} on. After the three capacitor voltages turn to equal, S_{3p} and S_{2p} will be turned on so that the converter can smoothly transfer to the 1X mode steady state operation in Fig. 2.

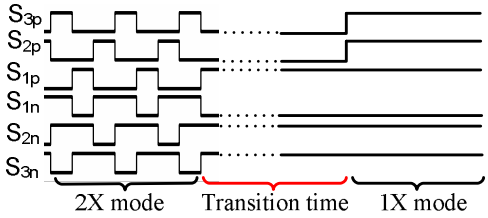

Fig.10. PWM signals during the transition from 2X to 1X

IV. Clamping Circuit

One of the challenges for the multi-level dc-dc converters in high power application is the high frequency spikes during the diode reverse recovery. They add significant stress and additional losses to the device, and also bring in EMI problems to the system. Therefore, a RCD clamping circuit as shown in Fig. 11 is proposed for this multilevel dc-dc topology. The basic principle is the same as that of the traditional RCD clamping circuit. When the switch is turned off, the current will be first diverted into the clamping

capacitor through the clamping diode. Then the clamping capacitor regenerates the energy back to the main capacitor through a resistor, as can be seen from the energy feedback loop for the clamping capacitors C_{1p} and C_{1n}. However, the other clamping cells in Fig. 11 make use of the switching devices in the main circuit to create the discharge loop. For instance, in Fig. 12(a), when the freewheeling diode in the switch S_{2n} turns off, the stray energy from the diode reverse recovery will flow into the clamping capacitor C_{2n}. When the switch S_{2n} is on, the stored energy will be fed back to C_1 through resistor R_{2n} and diode D_{d2n}. Such diodes in the discharge loop as D_{d2n} are added to guarantee the unidirectional current. In the same way, the clamping capacitor C_{3n} will get a chance to recover energy back to C_1 when the switches S_{2n} and S_{3n} are both conducting. It is noteworthy that in the boost mode operation, the actual conducting devices are the upper three freewheeling diodes in S_{xp} and the lower three IGBTs in S_{xn} (x=1, 2, 3), and vice versa in the buck mode operation. Nevertheless, the discharge current can still pass through either the IGBT or its freewheeling diode as any of them is carrying the load current.

The discharge loop for the clamping capacitor C_{3p} behaves in the same fashion, but there are two discharging states for C_{3p} as shown in Figs. 12(b) and (c). In the 1/3 switching period in Fig. 12(b), when the switches S_{2p} and S_{3n} are on, the captured energy in C_{3p} will flow to C_{out} through C_2, R_{3p} and D_{d3p}. In another 1/3 period in Fig. 12(c), the energy in C_{s3p} will flow to C_2 through C_1, R_{3p} and D_{d3p}, when the switches S_{3p} and S_{2n} are on.

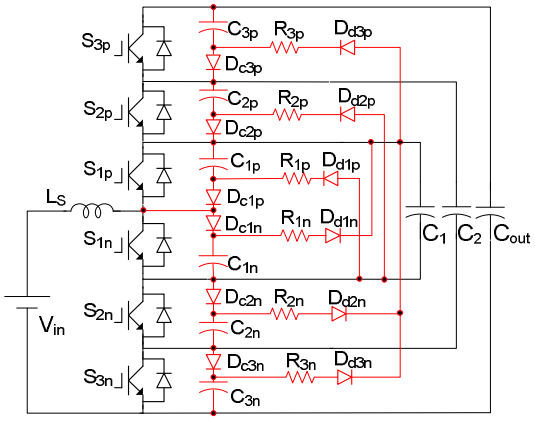

Fig.11. The clamping circuit

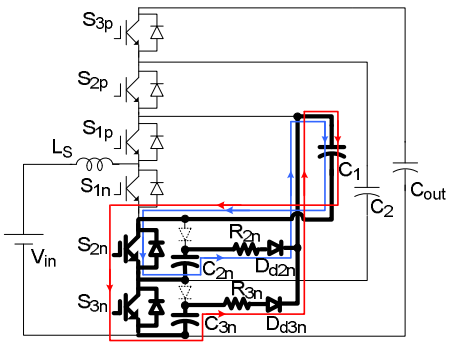

(a)

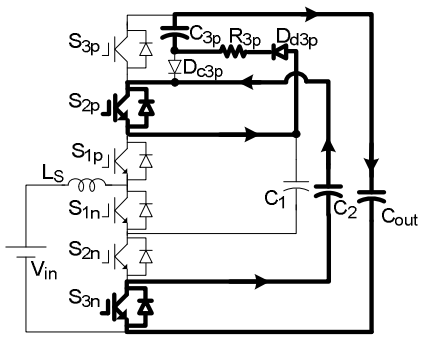

(b)

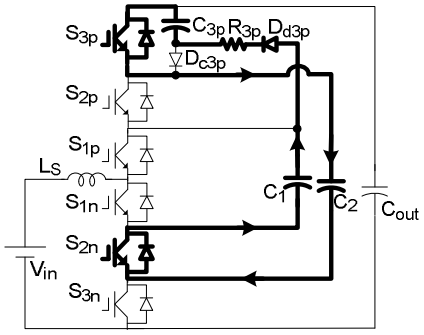

(c)

Fig.12. Typical discharge loops: (a) The discharge loop for S_{2n} and S_{3n}. (b) The discharging state I for S_{3p}. (c) The discharging state II for S_{3p}.

V. Experimental Results

A 55 kW prototype was built to verify the functionality. Fig.14 shows the final assembly based on the 3-D design in Fig. 13. The dimension is $27.2\times24.4\times8.8$ cm^3 and its weight is around 5.6 kg. The switches used are integrated in an IPM module PM600CLA600. The capacitors for C_1 and C_2 are 500μF and 240μF film capacitors respectively. The output capacitor consists of 40 uF film capacitors from the 3X dc-dc converter and an 820 uF capacitor bank that is to mimic the dc link capacitor shared between the dc-dc converter and the subsequent inverter. A 5 uH inductor is used in the experiment. In the hybrid electric vehicles, it is reasonable to take the advantage of the parasitic inductance in the battery and in the cable connecting the converter to the battery. In some hybrid electric vehicles, the battery is located about 2~3 meters away from the converter. The converter operates at 8 kHz in 3X mode and 12 kHz in 2X mode in steady state and it works at 20 kHz during the transition to limit the inrush current. The complex logic for duty ratio and frequency control in steady state and transient operation is implemented by one CPLD chip XC95288XL.

Fig. 15 shows the waveforms in the steady state operation. A buck/boost converter switching at 1 kHz is used to as an electronic load. Fig. 15(a) shows the input/output voltage and current waveforms in 3X mode at the 55 kW peak power. Figs. 15(b) and (c) are the corresponding waveforms in 2X and 1X modes at their 30 kW peak power. The output/input voltage ratio is lower than nX because of the device voltage stress and dead time as discussed in [4]. Fig.16 shows the converter

performance during voltage ratio change transition, in which the converter is loaded with a 30 Ohm resistor bank. As can be seen, in all cases the transient current is well limited. Fig. 17 shows the measured efficiency at different output power in nX mode. The overall efficiency in the 30 kW continuous power range is over 97%.

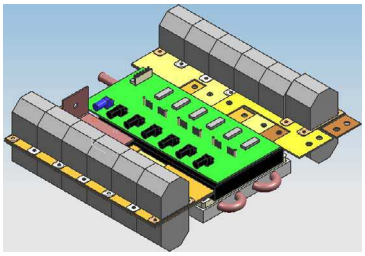

Fig. 13. 3-D design

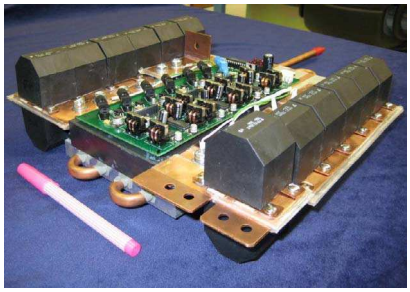

Fig. 14. The 55 kW dc-dc prototype

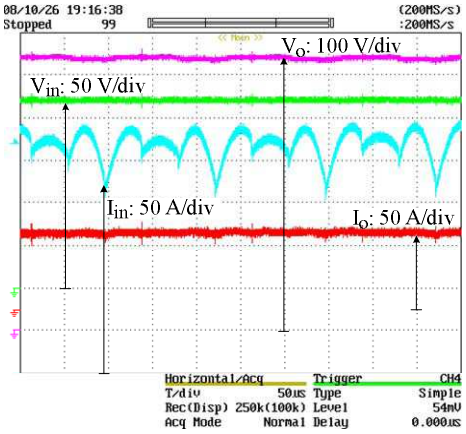

(a)

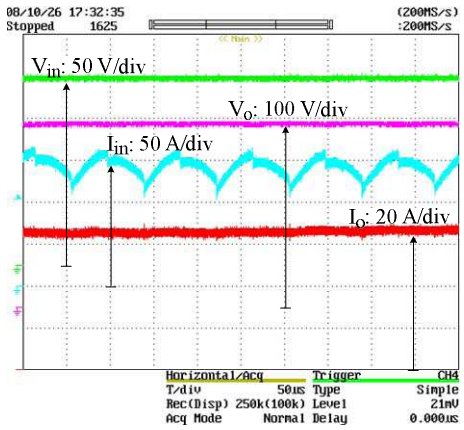

(b)

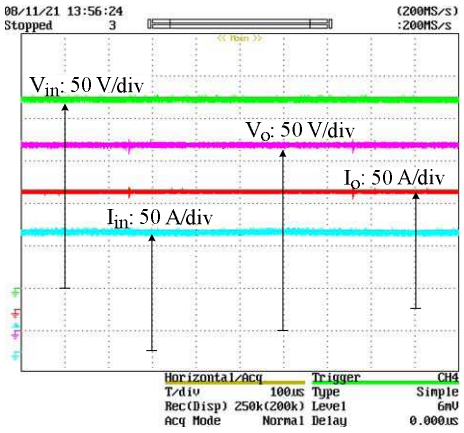

(c)

Fig. 15. Waveforms in steady state operation: (a) 3X boost mode at 55 kW output. (b) 2X boost mode at 30 kW output. (c) 1X boost mode at 30 kW output

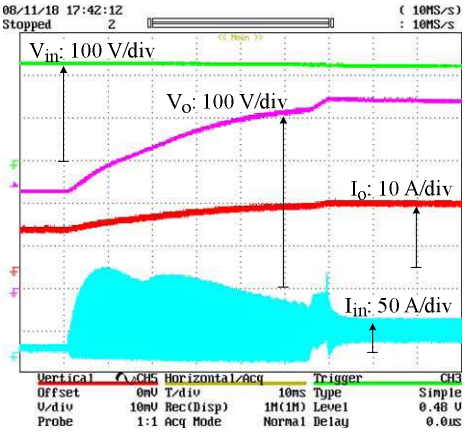

(a)

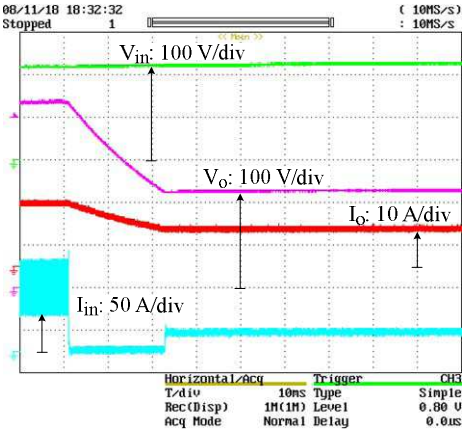

(b)

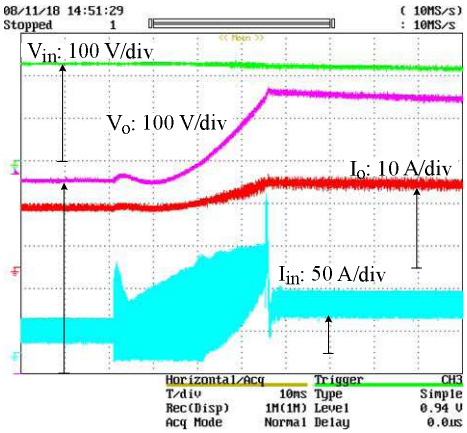

Fig. 16. Waveforms of the nX mode transition: (a) Transition from 1X to 2X. (b) Transition from 2X to 1X. (c) Transition from 2X to 3X. (d) Transition from 3X to 2X.

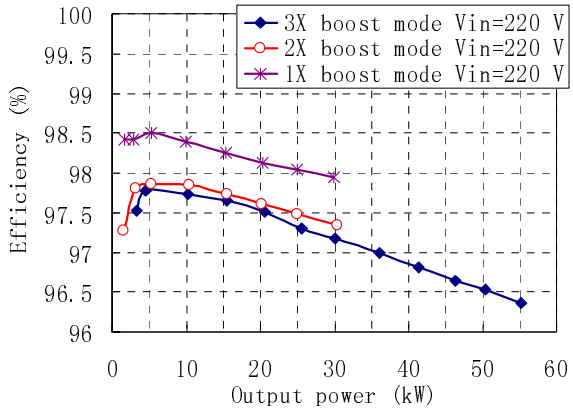

Fig.17. Efficiency of the 55 kW prototype

Compared with the conventional switched capacitor converters, the 3X multiplier/divider realizes three output/input voltage ratios by minimum number of capacitors and switching devices with the lowest voltage stresses. By the combination of three output voltage ratios in the dc-dc converter and the continuous adjustment of the modulation index, the inverter can operate in its high efficiency region. The dc-dc converter can be made more compact by using customized capacitors and heat sink. There is still great potential to make it even lighter by replacing the film capacitors with multilayer ceramic capacitors (MLCC), as nowadays some medium-voltage MLCCs already have several tens of microfarad capacitance and comparable ampere ripple current capability.

VI. Conclusion

A 3X dc-dc multiplier/divider with three variable output/input voltage ratios is presented in this paper. The transient current is well under control with the help of the duty ratio variation and switching frequency control. The proposed principle of the clamping circuit can serve as an example of addressing the high frequency spikes in multi-level converters. The experimental results of a 55 kW prototype in steady state and transient operation validate the operating principle. The efficiency testing results demonstrate its potential for high temperature HEV systems.

References

[1] F. Z. Peng, F. Zhang, Z. Qian, "A novel compact dc-dc converter for 42V systems," IEEE Power Electronics Specialists Conference, pp. 33-38, June 2003.

[2] F. Zhang, F. Z. Peng, Z. Qian, "study of multilevel converters in dc-dc application," IEEE Power Electronics Specialists Conference, pp. 1702-1706, June 2004.

[3] Z. Pan, F. Zhang, and F. Z. Peng, "Power losses and efficiency analysis of multilevel DC-DC converters," in Proc. IEEE Appl. Power Electron. Conf., Mar. 2005, pp. 1393–1398

[4] M. Shen; F. Z. Peng; L. M. Tolbert, "Multilevel dc-dc power conversion system with multiple dc sources", IEEE Transactions on Power Electronics, vol. 23, no. 1, pp. 420-426, Jan 2008.

[5] F. L. Luo and H. Ye, "Positive output multiple-lift push-pull switched capacitor Luo-converter," IEEE Trans. Ind. Electron., vol. 51, no. 3, pp. 594–602, Jun. 2004.

[6] K. K. Law, K. W. E. Cheng, and Y. P. B. Yeung, "Design and analysis of switched-capacitor-based step-up resonant converters," IEEE Trans. Circuits Syst. I, vol. 52, no. 5, pp. 943 - 948, May 2005.

[7] F. H. Khan, L. M. Tolbert, "Universal multilevel dc-dc converter with variable conversion ratio, high compactness factor and limited isolation feature", in Proc. IEEE Appl. Power Electron. Conf., Feb, 2008, pp. 17-23.

[8] B. Arntzen and D. Marksimovic, "Switched capacitor dc–dc converters with resonant gate drive," IEEE Trans. Power Electron., vol. 13, no. 5, pp. 892–902, Sep. 1998.

[9] W. Harris and K. Ngo, "Power switched-capacitor dc-dc converter, analysis, and design," *IEEE Trans. Aerosp. Electron. Syst.*, vol. 33, no. 2, pp. 386–395, Apr. 1997.